

Article

A New CPW-Fed Diversity Antenna for MIMO 5G Smartphones

Naser Ojaroudi Parchin ^{1,*}, Haleh Jahanbakhsh Basherlou ², Yasir I. A. Al-Yasir ¹, Ahmed M. Abdulkhaleq ^{1,3}, Mohammad Patwary ⁴ and Raed A. Abd-Alhameed ¹

¹ Faculty of Engineering and Informatics, University of Bradford, Bradford BD7 1DP, UK; Y.I.A.Al-Yasir@bradford.ac.uk (Y.I.A.A.-Y.); R.A.A.Abd@bradford.ac.uk (R.A.A.-A.)

² Bradford College, Bradford BD7 1AY, UK; Hale.Jahanbakhsh@gmail.com (H.J.B.)

³ SARAS Technology Limited, Leeds LS12 4NQ, UK; A.Abd@sarastech.co.uk (A.M.A)

⁴ School of Computing and Digital Technology, Birmingham City University, Birmingham, UK; Mohammad.patwary@bcu.ac.uk (M.P.)

* Correspondence: N.OjaroudiParchin@Bradford.ac.uk; Tel.: +447341436156

Abstract: In this study, a new coplanar waveguide (CPW)-fed diversity antenna design is introduced for multiple-input-multiple-output (MIMO) smartphone applications. The diversity antenna is composed of a double-fed CPW-fed antenna with a pair of modified T-ring radiators. The antenna is designed to cover the frequency spectrum of commercial sub-6 GHz 5G communication (3.4–3.8 GHz and 3.8–4.2 GHz). It also provides high isolation, better than -16 dB, without an additional decoupling structure. It offers good potential to be deployed in future smartphones. Therefore, using four pairs of the proposed diversity antennas, characteristics and performance of an 8-port 5G smartphone antenna are investigated. Due to compact size and also placement of the elements, the presented CPW-fed smartphone antenna array design occupies a very small part of the smartphone board. Its operation band spans from 3.4 to 4.4 GHz. The simulated results agree well with measured results and the performance of the smartphone antenna design in the presence of user are given in the paper as well. The proposed MIMO design provides not only sufficing radiation coverage supporting different sides of the mainboard but also the polarization diversity.

Keywords: 5G technology; CPW-fed antenna; diversity antenna; future smartphones; MIMO systems;

1. Introduction

With the development and standards' building of the fifth-generation (5G) mobile communication, more and more researches have been carried into related technologies with the hope of higher transmission rate, lower cost and higher gain [1–3]. Multiple-input-multiple-output (MIMO) technology is a key feature to realize a higher transmission rate [4]. By using MIMO technology, multiple independent channels can be achieved on the original spectrum by diversity method and reduce multipath fading, so as to improve the data transmission rate. MIMO antenna is a significant facility to improve the channel capacity of the MIMO system [5–8]. 2×2 MIMO systems are successfully employed for 4G mobile networks and a large number of antenna elements is expected to be applied for 5G communications [9–10].

Several kinds of 5G MIMO smartphone antennas have been put forward recently [11–25]. However, these MIMO antenna designs either suffer from narrow frequency bandwidth or occupy a huge space of smartphone mainboard. Furthermore, some of the reported designs use uniplanar radiators that confront difficulty in fabrication and integration with the 5G smartphone circuit. In the designs of many MIMO antennas, it's common to avoid placing elements in parallel and choose to place them vertically, which can avoid strong mutual couplings caused by the same polarization mode. However, in this paper, the antenna elements are perpendicular to each other and parallel to

each other to exhibit diversity function. In addition, the T-shaped strip of the antenna configuration can act as a decoupling structure. Furthermore, due to compact size and also placement of the antenna, the proposed MIMO desi occupy a very small part of the smartphone PCB board. Therefore, the proposed MIMO antenna achieves not only low mutual couplings but also small clearance.

The antenna elements of the MIMO design are fed using the coplanar waveguide feeding mechanism to operate at sub-6 GHz 5G communication (3.4-3.8 GHz and 3.8-4.2 GHz) [26]. Compared with probe-fed and microstrip-fed antennas, CPW-fed antenna can easily achieve the wideband impedance matching [27-28]. Therefore, CPW-fed antennas are widely used and becoming increasingly popular in wireless applications owing to their attractive features such as compact-size, conformal, light in weight, easy to fabricate and integrate with wireless communication systems. [29-30]. The paper is organized as follows: the design and characteristics of the diversity antenna element are represented in Section II. Section III discusses the MIMO performance and radiation characteristics of the proposed 5G smartphone antenna array. Section IV investigates the radiation behavior of the designed smartphone antenna array in the vicinity of the user. Section V gives a conclusion of this paper.

2. The Proposed CPW-Fed Diversity Antenna

The characteristics of the single-element diversity antenna have been discussed in this section. Its structure is shown in Fig. 1 (a). It is shown that the schematic of the diversity antenna contains a pair of modified CPW-fed T-ring resonators. As seen, the proposed antenna is designed on one-side of the FR4 dielectric. Figure 1 (b) depicts the S-parameters of the proposed CPW-fed diversity antenna. As illustrated, the designed antenna provides a wide operation band of 3.2-4.4 GHz, supporting both target bands including 3.4-3.8 and 3.8-4.2 GHz. It should be noted that the arrow-shaped strip of the design, placed between the elements, can act as a decoupling structure and increase the isolation between the antenna ports. Therefore, the mutual coupling (S_{21}/S_{21}) is successfully reduced. As can be observed, better than -15 dB (with -20 dB value at the center frequency (4 GHz)) has been achieved for the designed diversity antenna. The characteristics of the antenna are investigated using CST software [31]. The detailed dimensions of the designed CPW-fed diversity antenna are shown in Table 1.

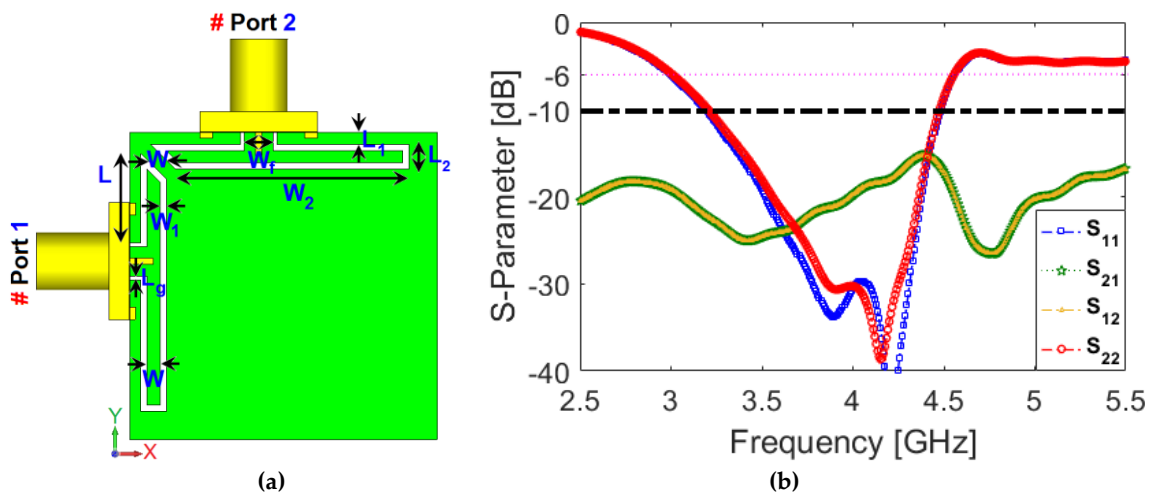


Figure 1. (a) Geometry of the CPW-fed diversity antenna and (b) its simulated S-parameters.

Table 1. The dimension of the diversity antenna.

Parameter	Value (mm)	Parameter	Value (mm)	Parameter	Value (mm)	Parameter	Value (mm)
W	1.1	W ₁	0.5	W ₂	19	W _f	2.4
L	7	L ₁	1	L ₂	2	L _g	0.25

The frequency behavior of the proposed diversity antenna is very flexible. In Fig. 2 the impedance matching and frequency tuning of the antenna are discussed. Figure 2 (a) illustrates the S_{11} and S_{21} characteristics versus different values of W_2 . As seen, when its value increases from 17 mm to 21 mm, the lower and upper operation frequencies of the antenna decrease from 3 to 3.4 GHz and 4.5 to 4.8 GHz, respectively. In addition, as can be observed, the S_{21} function of the diversity antenna tunes by changing the value of W_2 . Figure 2 (b) investigate the impedance matching function of the antenna for various values of L_2 : when its size of changes from 2.75 to 1.75 mm, the matching characteristic of the diversity antenna varies from -14 dB to less than -30 dB. However, unlike Fig. 2 (a), the S_{21} is almost constant with an insignificant variation.

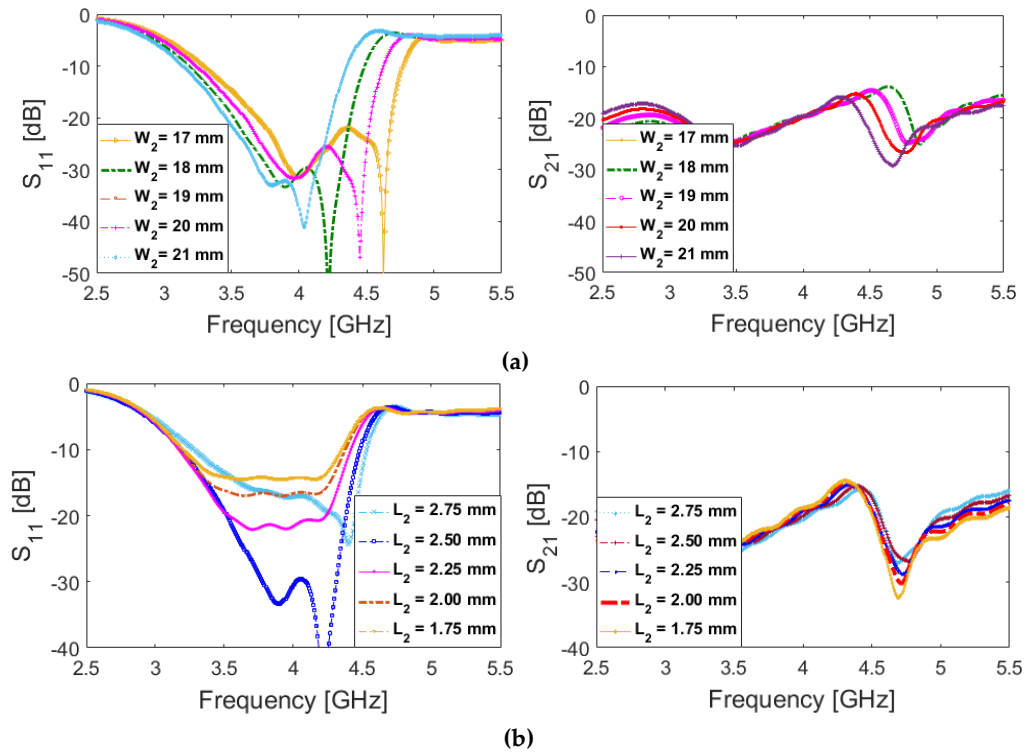


Figure 2. S_{11}/S_{21} results of the diversity antenna for various values of (a) W_2 and (b) L_2 .

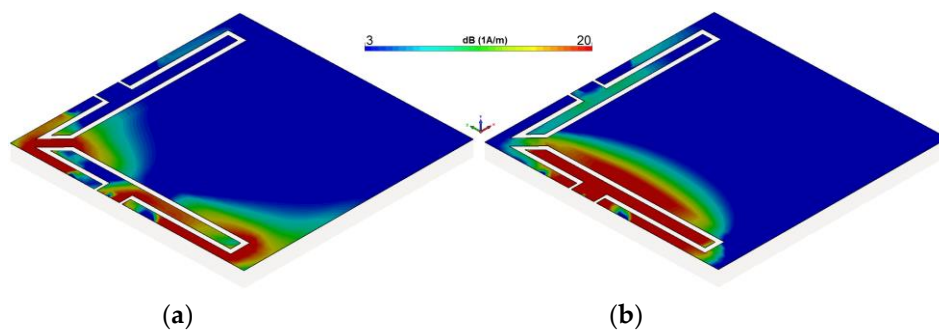


Figure 3. The current densities of the diversity antenna design at 4 GHz for (a) port 1 and (b) port 2.

In order to have a better illumination about the working mechanism of the CPW-Fed, its simulated current distributions at 3.8 GHz and 4.2 GHz are shown in Fig. 3, respectively. As shown at 3.8 GHz, the current is mainly distributed near the arrow strip and outer of the modified T-ring resonator, which verifies the role of the strip in creating a new resonance at 3.8. While at 4.2 GHz, the currents are mainly concentrated inside of the modified T-ring slot [31-32]. The radiation patterns of the diversity antenna for each exciting port at 4 GHz (center frequency of the antenna operation band) are plotted in Fig. 4. It is shown that well-defined polarization and pattern diversity is obtained for

the antenna. The radiation patterns of the antenna are symmetrical covering top/bottom sides of the substrate and providing similar radiation behavior with gain vale of 4 dBi. The fundamental radiation characteristics of the diversity antenna are also given in Fig. 5 within the range of 3.4-4.4 GHz (with 0.1 GHz/step). As illustrated in Fig. 5, the antenna exhibits high efficacies over its 1 GHz impedance bandwidth. In addition, the antenna offers sufficient gain and directivity in the range of 3.4-4.4 GHz.

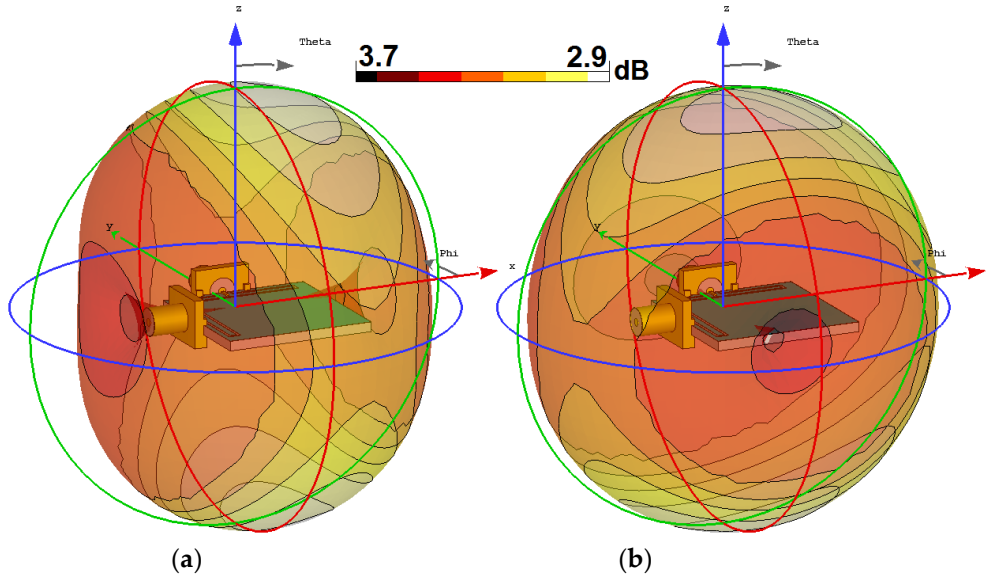


Figure 4. Radiation patterns of the CPW-fed diversity antenna at 4 GHz from (a) port 1 and (b) 2.

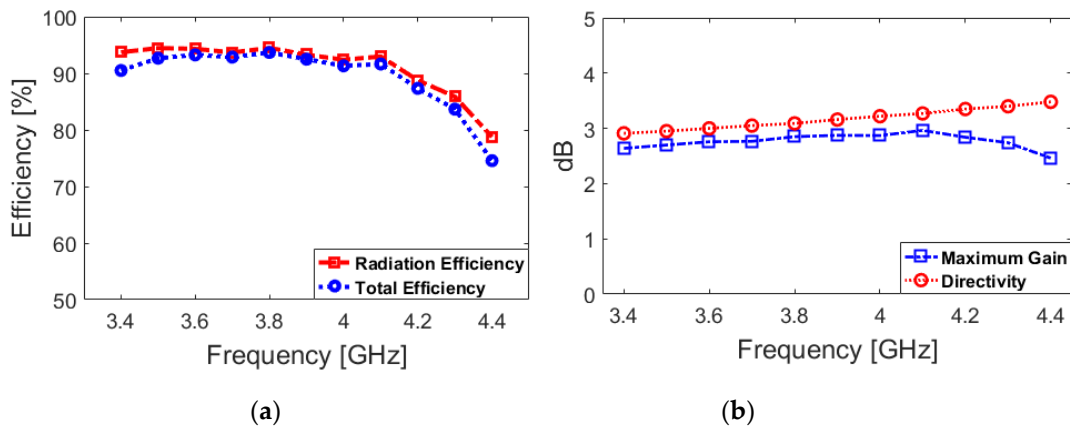


Figure 5. Simulated characteristics of the CPW-fed diversity antenna.

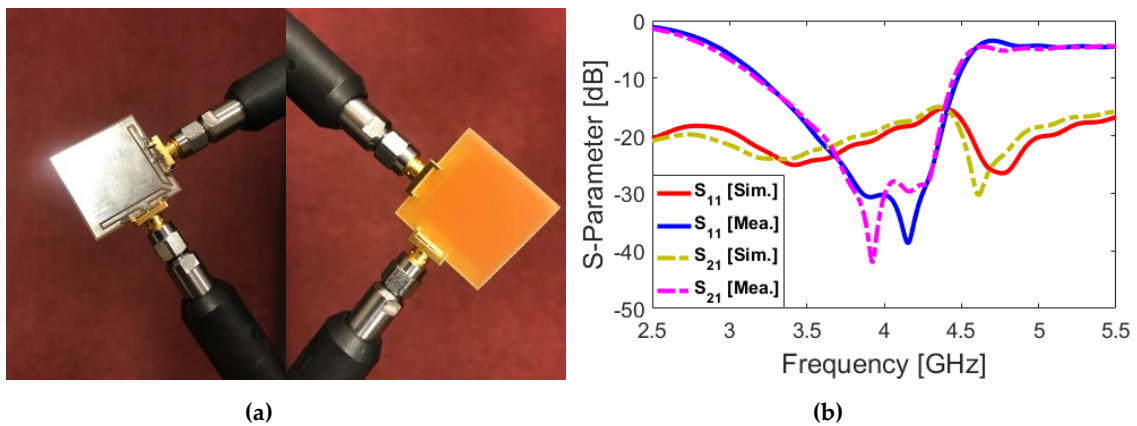


Figure 6. (a) Fabricated antenna's top/bottom sides and (b) its S-parameters.

A prototype of the design was fabricated and its S parameters were tested. In order to verify the simulated S-parameter results mentioned above, the single-element diversity antenna was fabricated and measured. A vector network analyzer was used to measure the antenna in our research. The fabricated dual-port antenna and the measured results of S-parameters are given in Fig. 6 (a) and (b). As illustrated in Fig. 6 (b), the measured results of the diversity antenna based on FR-4 are very close to the simulated results values within 2.5-5.5 GHz: it provides a quite good impedance bandwidth ($S_{11} < -10$ dB within 3.2-4.4 GHz), and its mutual coupling (S_{21}) is less than -15 dB.

The total active reflection coefficient (TARC), envelope correlation coefficient (ECC), and Diversity gain (DG) characteristics are important parameters to be considered in diversity/MIMO antennas and can be calculated using the below formulas [33-35].

$$TARC = -\sqrt{\frac{(S_{11} + S_{12})^2 + (S_{21} + S_{22})^2}{2}} \quad (1)$$

$$ECC = \frac{|S_{11}^* S_{21} + S_{12}^* S_{22}|^2}{(1 - |S_{11}|^2 - |S_{12}|^2)(1 - |S_{21}|^2 - |S_{22}|^2)^*} \quad (2)$$

$$DG = 10\sqrt{1 - (ECC)^2} \quad (3)$$

Figure 7 represents the calculated TARC, ECC, and DG characteristics for the proposed dual-port diversity antenna. As it shows in Figs. 7 (a) and (b), the TARC and ECC results of this diversity antenna are very low within the band, which means the antenna is competent for diversity reception/transmission in the MIMO channels [33]. In addition, as can be observed from Fig. 7 (c), the DG function of the design is more than 9.97 dB over the entire band.

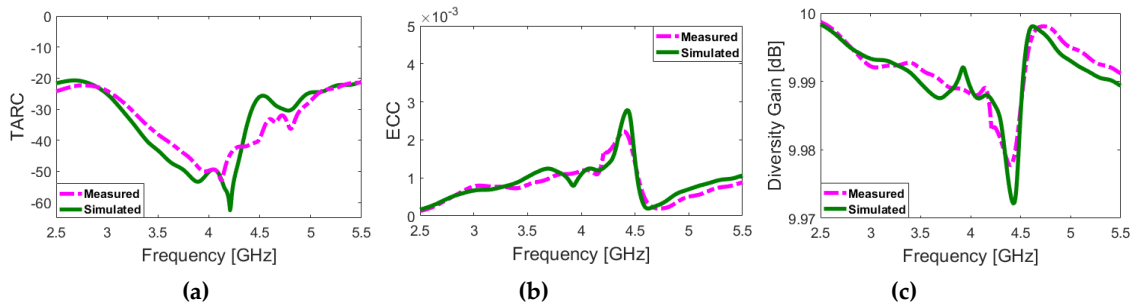


Figure 7. Calculated (a) TARC, (b) ECC, and (c) DG characteristics of the CPW-fed diversity antenna.

3. Mobile-Phone Antenna Design

Four pairs of the modified CPW-fed diversity antenna mentioned above were placed in different corners of the smartphone board to form an eight-port MIMO antenna with a standard size of $150 \times 75 \times 1.6$ mm³. Its structure is shown in Fig. 8. As can be observed, due to compact size and also placement of the CPW-fed ring antenna, the proposed MIMO design occupies a very small part of the board.

Figure 9 shows the S-parameters of the CPW-fed MIMO smartphone antenna. It can be observed from Fig. 9 (a) that all antenna elements exhibit good S_{nn} results covering 3.4-4.4 GHz. The isolations between ports are shown in Fig. 9 (b). As seen, the S_{mn} results of the antenna ports are less than 16 dB within 3.4-4.4 GHz. That's because the main radiation elements have strong mutual couplings between the adjacent ports. It should be also noted that due to effect of MIMO configuration and also big ground plane of the smartphone board, the lower operation frequency shifted from 3.2 to 3.4 GHz. However, it still covers the target 5G bands including 3.4-3.8 GHz and 3.8-4.2 GHz.

Figure 10 plots the radiation patterns at the middle frequency (4 GHz) for the first CPW-fed diversity antenna (with ports 1&2) mounted onto the smartphone PCB. As seen, the radiation patterns are symmetrical covering top/bottom sides of the substrate and providing similar radiation behavior with gain vale of 4 dBi.

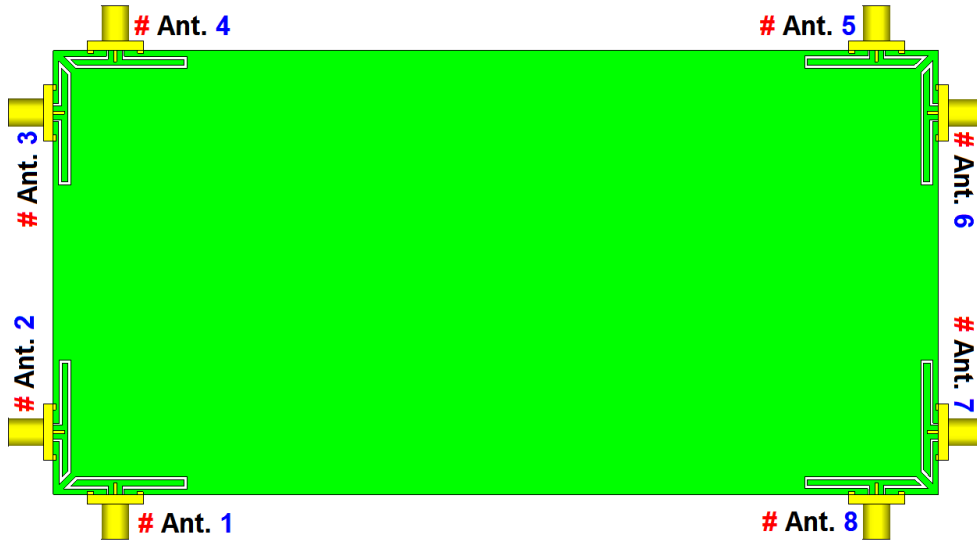


Figure 8. Schematic of the CPW-fed eight-port 5G smartphone antenna.

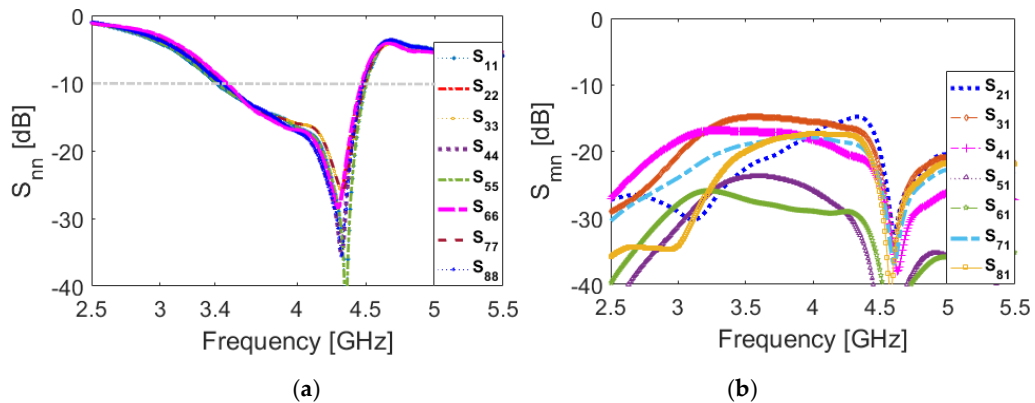


Figure 9. The simulated (a) S_{nn} and (b) S_{mn} results.

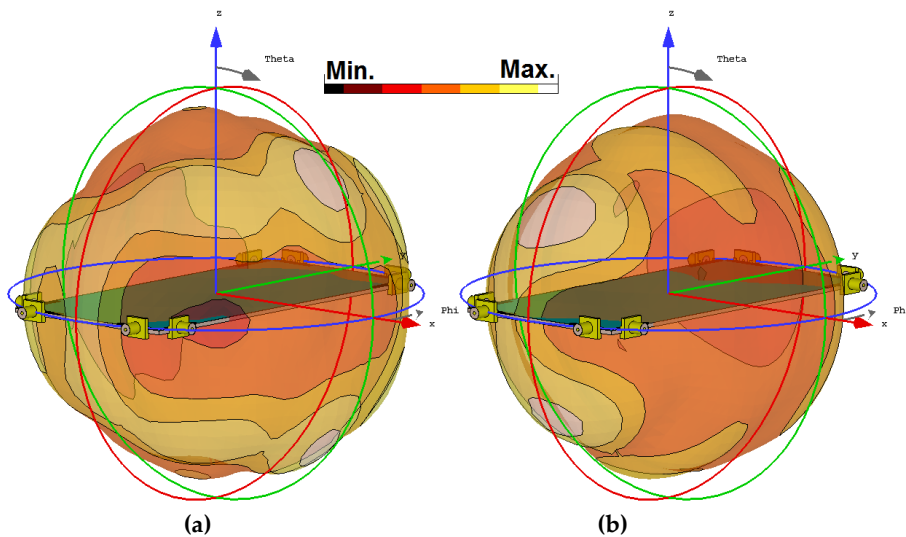


Figure 10. Radiation patterns of the dual-port diversity resonator from (a) port 1 and (b) port 2.

3D patterns of antenna radiations at 4 GHz for each feeding port have been illustrated in Fig. 11. It can be observed that the CPW-fed resonators not only can cover different sides of the mobile-phone board but also support different polarizations which is a unique function for MIMO design [36-37]. In addition, good gain values varying from 4.6 to 5.15 dBi are achieved for the resonators. The efficiencies (radiation and total) of the CPW-fed ring slot resonators are also given in Fig. 12. It is evident that high efficiencies with slight variations are achieved within the range of 3.4-4.4 GHz: more than 80% radiation and 70% total efficiencies were observed for the CPW-fed elements of the proposed MIMO design.

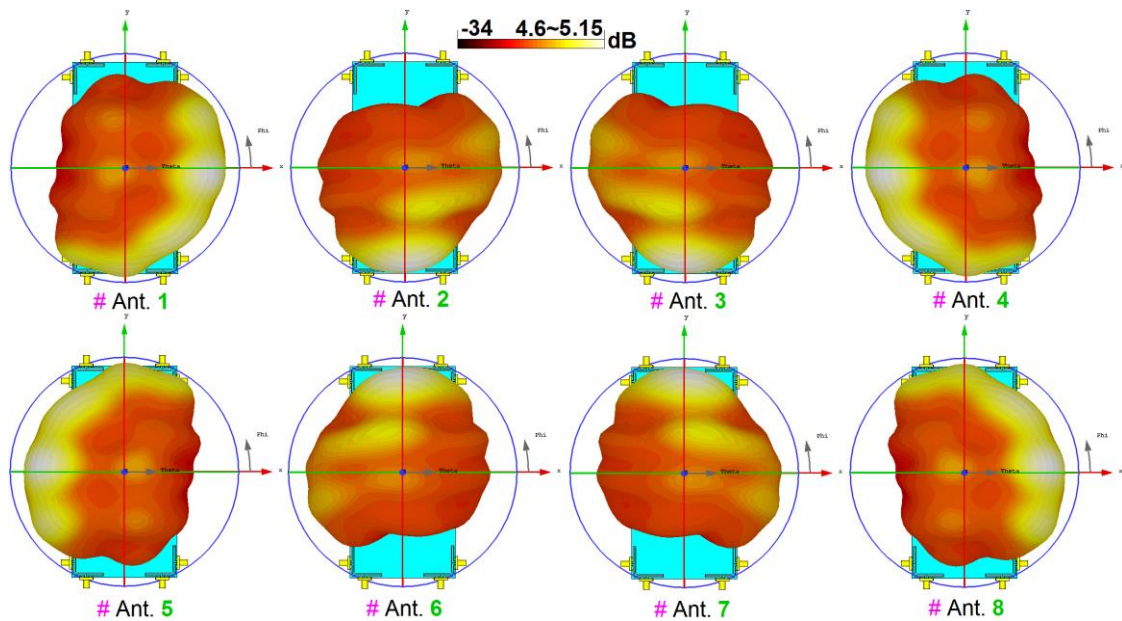


Figure 11. 3D radiation patterns at center frequency (4 GHz).

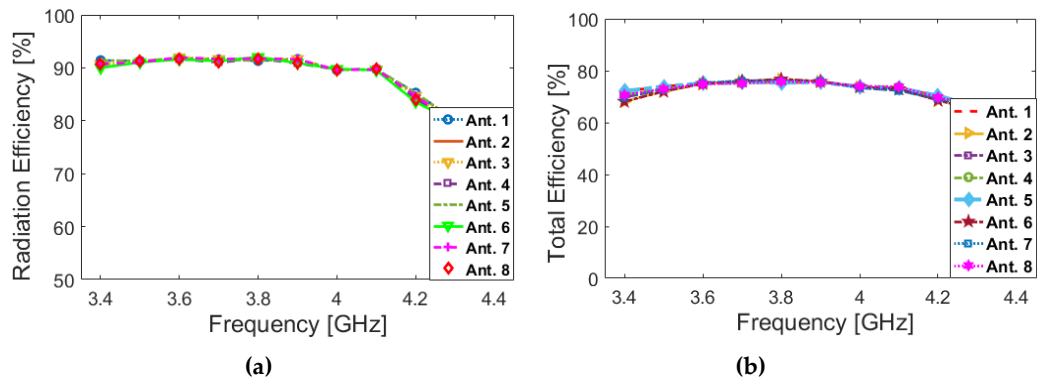


Figure 12. (a) Radiation and (b) total Efficiencies of the antenna elements (Ant. 1–Ant. 8) for the proposed design.

A prototype of the 5G smartphone antenna design was fabricated and fed for measurements, as illustrated in Fig. 13. In order to verify the simulated results of the smartphone antenna, mentioned above, the S-parameter and radiation patterns were measured. However, due to similar placements and also the performances of the CPW-fed antenna pairs, the properties of the smartphone antenna design for port 1 and 2 are measured and compared in the following. A vector network analyzer and antenna chamber room were used in the measurement process of our research.

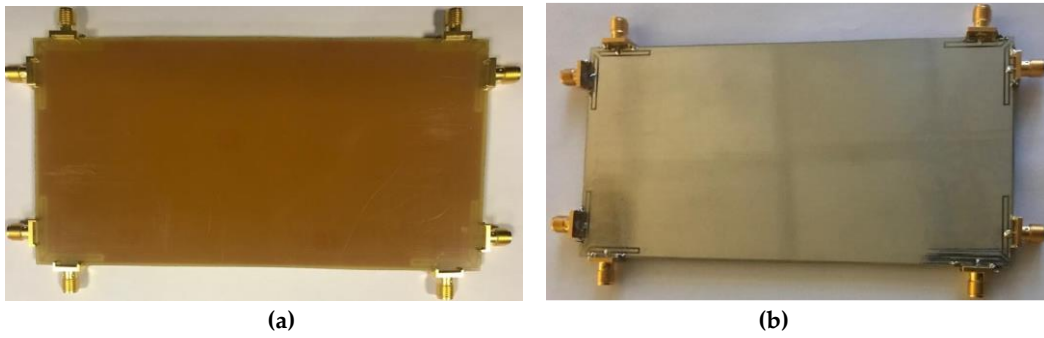


Figure 13. (a) Front and (b) back views of the fabricated sample.

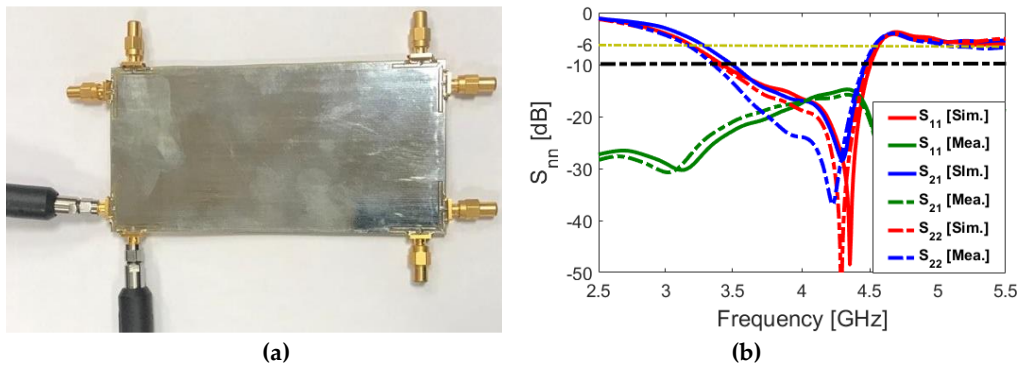


Figure 14. (a) Feeding mechanism and (a) S-parameters of adjacent CPW-fed elements for the 5G smartphone antenna.

The feeding mechanism of the design is shown in Fig. 14 (a). During the measurements, in order to avoid unwanted mutual effects, 50-Ω RF loads are installed for the elements not under test. The measured and simulated results of the S-parameters are compared in Fig. 14 (b). As seen, the measured results are in good agreement with the simulated results to cover the required operation band: a quite good impedance bandwidth ($S_{11} < -10$ dB within 3.4-4.4 GHz), and mutual coupling ($S_{22} < -15$ dB) are obtained for the smartphone antenna design. Measured and simulated radiation patterns are shown in Fig. 15. When measuring radiation patterns, we keep one port excited and another one loaded with a 50-Ω load. In the measurement of radiation patterns, the smartphone MIMO antenna is used as the receiver, and a horn antenna is used as the transmitter. As can be observed from Figs. 15 (a) and (b), the sample smartphone antenna prototype offers good quasi-omnidirectional radiation patterns with acceptable agreement between simulations and measurements [38-40].

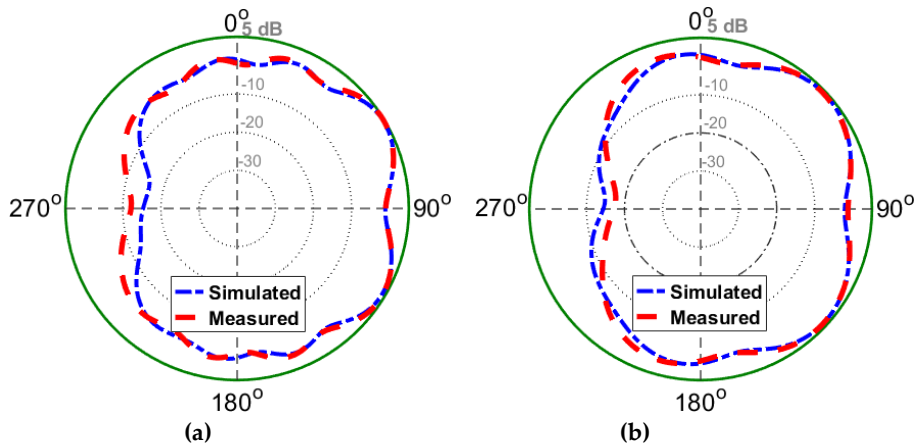


Figure 15. 2D radiation patterns (a) Ant.1 and (b) Ant.2.

Table 2 provided a comparison between the presented smartphone array antenna and some other reported smartphone array [11-25]. As can be observed, compared with the recently proposed 5G MIMO smartphone antennas with planar and uniplanar structures, our antenna has a better performance in terms of impedance match and bandwidth, and its clearance size keeps at a satisfactory level, as shown in Table 2. The proposed design achieves not only around 1 GHz impedance bandwidth but also sufficient mutual couplings, better than -15 dB. Besides, unlike the reported 5G antenna design, our antenna is implemented in one-side of the smartphone mainboard using CPW-fed technology which makes it easy to fabricate and integrate with the circuit. It is apparent that all the listed antennas have double-sides or uniplanar configuration. In addition, due to the small clearance of the proposed smartphone antenna, its fundamental radiation properties in data and talk modes are not reduced significantly, as discussed in the following.

Table 2. Comparison between our design and the referenced 5G smartphone antennas.

Reference	Design Type	Bandwidth (GHz)	Efficiency (%)	Size (mm ²)	Isolation (dB)	ECC
[11]	Gap-Coupled IFA	3.4-3.6	-	150 × 75	15	< 0.02
[12]	Inverted-F	3.4-3.6	55-60	100×50	10	-
[13]	Patch-Slot	3.55-3.65	52-76	150 × 75	11	-
[14]	Monopole	3.4-3.6	35-50	150 × 75	11	< 0.40
[15]	Spatial-Reuse Antenna	3.4-3.6	40-70	150 × 75	12	< 0.2
[16]	Inverted-L Monopole	3.4-3.6	40-60	136 × 68	14	< 0.2
[17]	Inverted-F	3.4-3.6	-	120×70	20	-
[18]	Ring-Slot	3.4-3.8	60-75	150 × 75	15	< 0.01
[19]	Monopole	4.55-4.75	50-70	136 × 68	10	-
[20]	Tightly Arranged Pairs	3.4-3.6	50-70	150× 73	17	< 0.07
[21]	Wave-Guide	3.4-3.6	50-80	150 × 75	15	< 0.2
[22]	Monopole	3.4-3.6	60-70	150 × 75	18	< 0.015
[23]	Diamond-shaped Slot	3.3-3.9	60-80	150 × 75	17	< 0.01
[24]	open-end slot	3.4-3.6	50-60	136 × 68	11	0.05
[25]	loop element	3.3-3.6	40	120×70	15	0.02
Proposed	CPW-Fed Diversity	3.4-4.4	65-80	150 × 75	16	< 0.005

4. User Impacts on the Performance of the CPW-fed Smartphone Antenna Array

For smartphone antennas, it is indispensable to investigate the user-effect on the radiation performance of the antenna [41-42]. Different usage postures in data-mode and talk-mode are considered in this section. Figure 17 represents S_{nn} and efficiency results of the 5G antenna in data mode with different placement modes for right/left hands touching top/bottom sides of the smartphone. It can be observed similar characteristics are achieved for different data-mode scenarios. This is mainly due to symmetrical configuration and similar placements of the CPW-fed antenna pairs. In addition, as shown in Fig. 17, the S_{nn} results of all elements is not influenced significantly and still could cover the desired operation band. Some variation is discovered for the elements which partially covered with the hand-phantom, due to its absorption. Furthermore, it is evident from Fig. 17 (c), a part of the radiation power of antenna is absorbed by the medium which causes some reduction in the efficiencies of the elements. However, the elements still provide around 40% and more total efficiencies within the 3.4-4.4 GHz operation band.

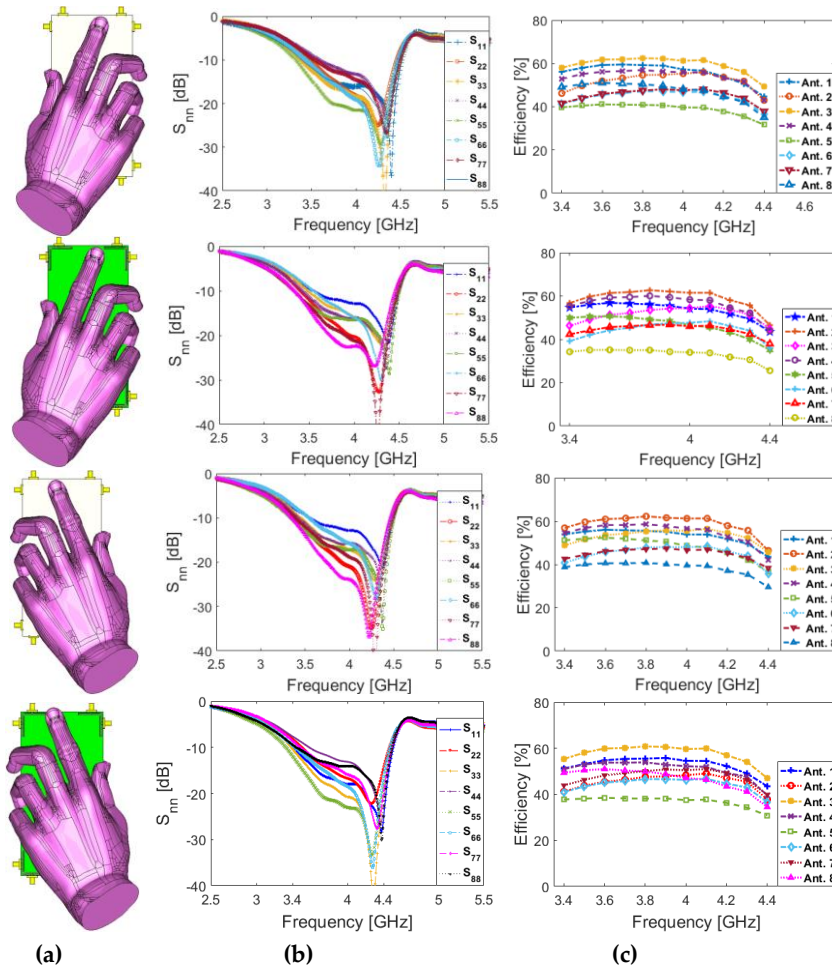


Figure 17. (a) Placement, (b) S_{nn} , and (c) total efficiencies for different data-mode scenarios.

Apart from the data-mode, discussed above, the characteristics of the CPW-fed resonators in Talk-mode are also investigated and represented in Fig. 18. It is evident the antenna elements work sufficiently and provide good S_{nn} and total efficiency results for different antenna elements. The radiation pattern results for the MIMO smartphone antenna in Talk-mode are shown in Fig. 18. As can be obviously realized from the simulation, the proposed CPW-fed MIMO antenna offers good radiation patterns in Talk-mode. In addition, the gain levels of the CPW-fed antenna resonators varies from 2 to 5 GHz. Compared with Fig. 8, the maximum reduction of antenna gain is observed for the elements closely spaced with the user head and hand. In general, the closer the distance between the antenna element and the user-hand/head is, the greater reduction on the gain and the efficiencies will be [43].

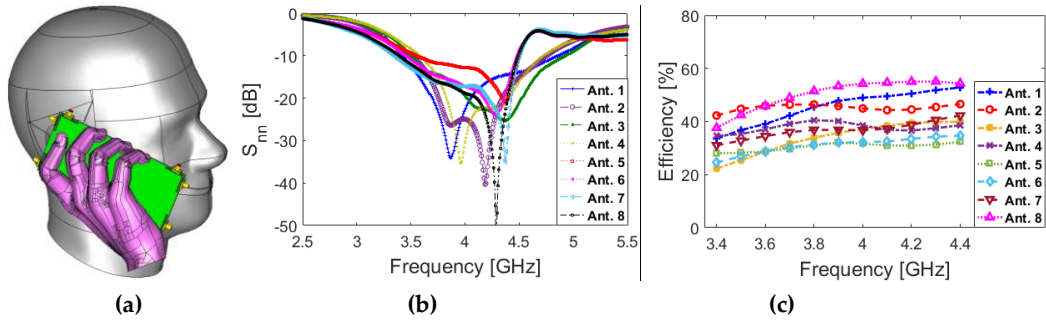


Figure 17. (a) Placement, (b) S_{nn} , and (c) total efficiencies for talk-mode.

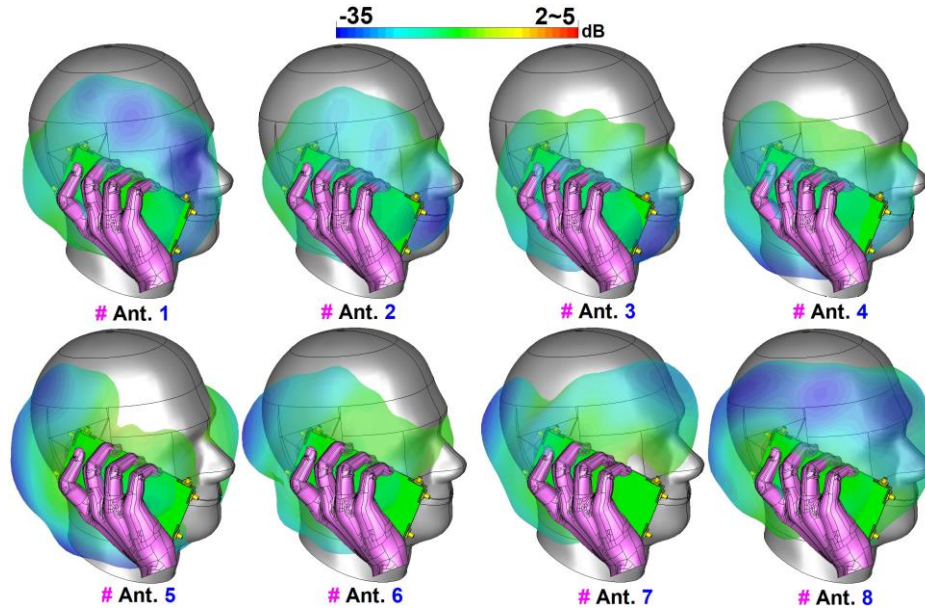


Figure 18. Radiation patterns in Talk-Mode.

The specific absorption rate (SAR) characteristic of the CPW-fed MIMO design is studied and represented in Fig. 19. It is shown that Ant. 3 causes the maximum SAR value (2.1) and the minimum SAR value (0.7) is observed from Ant. 7. Therefore, it can be concluded that the closer the distance between antenna elements and the user-head leads to a maximum SAR value and vice versa [44-45].

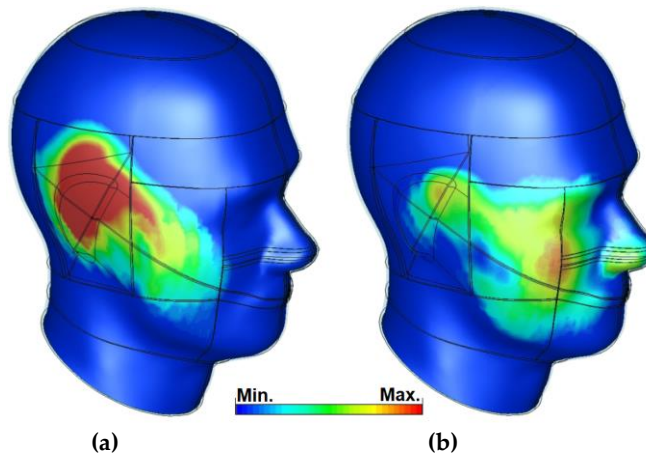


Figure 19. SAR investigations for (a) Ant. 3 and (b) Ant. 7.

The S_{nn} ($S_{11} \sim S_{88}$) and efficiency characteristics of the CPW-fed MIMO smartphone antenna in the presence of battery, speaker, camera, USB connector, and LCD screen are investigated and illustrated in Fig. 20. It is found that the designed CPW-fed MIMO antenna provides sufficient S_{nn} and efficiencies supporting 3.4-4.4 GHz band.

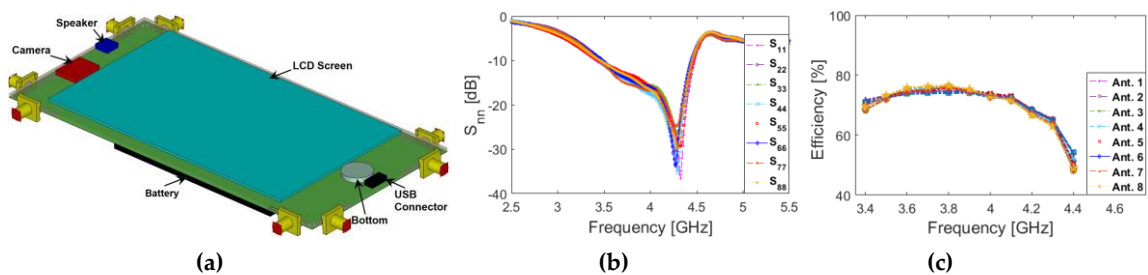


Figure 20. (a) Schematic, (b) S_{nn} and (b) in the presence of the smartphone components.

5. Conclusions

A smartphone array antenna design with new double-fed CPW-fed resonators is introduced for sub 6 GHz 5G applications. The structure of the CWP-fed element consists of two closely-spaced modified T-ring radiators operating with the frequency band 3.3-4.4 GHz. Four pairs of the CPW-fed diversity antennas are placed at four corners of the smartphone board to form an 8×8 MIMO antenna. Fundamental characteristics and MIMO performance of the design are studied and sufficient results are achieved. Simulated and experimental results are provided to validate the usefulness of the designed smartphone antenna array for 5G mobile communications.

Author Contributions: writing—original draft preparation, N.O.P., H.J.B., M.P., Y.I.A.A.-Y., and R.A.A.-A.; writing—review and editing, N.O.P. and R.A.A.-A.; investigation, N.O.P., H.J.B., M.P., Y.I.A.A.-Y.; resources, N.O.P., R.A.A.-A., M.P. and; For other cases, all authors have participated.

Funding: This project has received funding from the European Union’s Horizon 2020 research and innovation programme under grant agreement H2020-MSCA-ITN-2016 SECRET-722424.

Acknowledgments: The authors wish to express their thanks to the support provided by the innovation programme under grant agreement H2020-MSCA-ITN-2016 SECRET-722424.

Conflicts of Interest: The authors declare no conflict of interest.

References

1. Nadeem, Q.U.A.; *et al.* Design of 5G full dimension massive MIMO systems. *IEEE Trans. Commun.* 2018, 66, 726–740.
2. Ojaroudiparchin, N.; Shen, M.; and Pedersen, G. F. Multi-layer 5G mobile phone antenna for multi-user MIMO communications. in *Proc. 23rd Telecommun. Forum Telfor (TELFOR)*, Nov. 2015, pp. 559–562
3. Osseiran, A.; *et al.* Scenarios for 5G mobile and wireless communications: the vision of the METIS project. *IEEE Commun. Mag.* 2014, 52, 26-35.
4. Yang, H.H.; Quel, Y.Q.S. Massive MIMO Meet Small Cell. *SpringerBriefs in Electrical and Computer Engineering*, 2017. DOI 10.1007/978-3-319-43715-6_2.
5. Ojaroudi, N. and Ghadimi, N. Design of CPW-fed slot antenna for MIMO system applications. *Microw. Opt. Technol. Lett.* 2014, 56, 1278- 1281.
6. Ojaroudi Parchin, N.; *et al.* Recent developments of reconfigurable antennas for current and future wireless communication systems. *Electronics* 2019, 8, 1-17.
7. Hussain, R.; Alreshaid, A.T.; Podilchak, S. K.; and Sharawi, M.S. Compact 4G MIMO antenna integrated with a 5G array for current and future mobile handsets. *IET Microw. Antennas Propag.* 2017, 11, 271-279.
8. Ojaroudi, N. *et al.* Quadband planar inverted-f antenna (PIFA) for wireless communication systems. *Progress In Electromagnetics Research Letters.* 2014, 45, 51- 56.
9. Chen, Q.; *et al.* Single ring slot based antennas for metal-rimmed 4G/5G smartphones. *IEEE Trans. Antennas Propag.* 2018, DOI 10.1109/TAP.2018.2883686
10. Ojaroudiparchin, N.; *et al.* Wide-scan phased array antenna fed by coax-to- microstriplines for 5G cell phones. *21st International Conference on Microwaves, Radar and Wireless Communications* 2016, Krakow, Serbia.
11. Liu, Y.; *et al.* MIMO antenna array for 5G smartphone applications. *13th European Conference on Antennas and Propagation (EuCAP 2019)*. 2019, Krakow, Poland.
12. Al-Hadi, A.A.; Ilvonen, J.; Valkonen, R.; Viikan, V. Eight-element antenna array for diversity and MIMO mobile terminal in LTE 3500MHz band. *Microwave Opt. Technol. Lett.* 2014, 56, 1323- 1327.
13. Ojaroudi Parchin. N. *et al.* Dual-polarized MIMO antenna array design using miniaturized self-complementary structures for 5G smartphone applications. *EuCAP Conference*, 2019, Accepted.
14. Wong, K. L.; *et al.* 8-antenna and 16-antenna arrays using the quad-antenna linear array as a building block for the 3.5-GHz LTE MIMO operation in the smartphone. *Microw. Opt. Technol. Lett.* 2016, 58, 174-181.
15. L. Chang, Y. *et al.* Polarization-orthogonal co-frequency dual antenna pair suitable for 5G MIMO smartphone with metallic bezels. *IEEE Trans. Antennas Propag.* 2019, 67, 5212–5220.
16. Abdullah, M.; *et al.* Eight-element antenna array at 3.5GHz for MIMO wireless application. *Progress In Electromagnetics Research C.* 2017, 78, 209-217.
17. Zhao, X.; Yeo, S.P.; Ong, L. C. Decoupling of inverted-F antennas with high-order modes of ground plane for 5G mobile MIMO platform. *IEEE Trans. Antennas Propag.*, 2018, 66, 4485–4495.

18. Parchin, N.O. *et al.* Eight-element dual-polarized MIMO slot antenna system for 5G smartphone applications. *IEEE Access*, 2019, 2019, 9, 15612-15622.
19. Xu, S.; Zhang, M.; Wen, H.; Wang, J. Deep-subwavelength decoupling for MIMO antennas in mobile handsets with singular medium. *Scientific Reports* 2017, 7, 12162.
20. Sun, L.; Feng, H.; Li, Y.; Zhang, Z. Compact 5G MIMO mobile phone antennas with tightly arranged orthogonal-mode pairs. *IEEE Trans. Antennas Propag.*, 2018, 66, 6364–6369.
21. Li, M.-Y.; *et al.* Tri-polarized 12-antenna MIMO array for future 5G smartphone applications. *IEEE Access* 2018, 6, 6160–6170.
22. Zhao, A.; Zhouyou R. Size reduction of self-isolated MIMO antenna system for 5G mobile phone applications. *IEEE Antennas and Wireless Propagation Letters*. 2019, 18, 152-156.
23. Parchin, N.O. *et al.* Mobile-phone antenna array with diamond-ring slot elements for 5G massive MIMO systems. *Electronics*, 2019, 8, 521, 1-17.
24. Abdullah, M. *et al.* High-performance multiple-input multiple-output antenna system for 5G mobile terminals. *Electronics*, 2019, 8, 1090, 1-16.
25. Jiang, W.; Liu, B.; Cui, Y.; Hu, W. High-isolation eight-Element MIMO array for 5G smartphone applications. *IEEE Access* 2019, 7, 34104–34112.
26. Statement: Improving Consumer Access to Mobile Services at 3.6 GHz to 3.8 GHz. Available online: <https://www.ofcom.org.uk/consultations-and-statements/category-1/future-use-at-3.6-3.8-ghz> (accessed on 21 October 2018).
27. Ojaroudi N. and Ghadimi, N. Dual-band CPW-fed slot antenna for LTE and WiBro applications. *Microw. Opt. Technol. Lett.*, vol. 56, pp. 1013- 1015, 2014.
28. Ojaroudi, N. Small microstrip-fed slot antenna with frequency band-stop function. 21th Telecommunications Forum. TELFOR 2013, 27 – 28 November, 2013, Belgrade, Serbia.
29. Ojaroudi, N. Design of microstrip antenna for 2.4/5.8 GHz RFID applications. German Microwave Conference, GeMic 2014, RWTH Aachen University, Germany, March 10-12, 2014.
30. Valizade, A., *et al.* Band-notch slot antenna with enhanced bandwidth by using Ω -shaped strips protruded inside rectangular slots for UWB applications. *Appl. Comput. Electromagn. Soc. (ACES) J.* 2012, 27, 816–822.
31. *CST Microwave Studio*; ver. 2018; CST: Framingham, MA, USA, 2018.
32. Al-Nuaimi, M. K. T.; Whittow, W. G. Performance investigation of a dual element ifa array at 3 ghz for mimo terminals. in *Antennas and Propagation Conference (LAPC)*, 2011, 1–5, Loughborough, UK.
33. Parchin, N.O. *et al.* Dual-band monopole antenna for RFID applications. *Future Internet* 2019, 11, 1-10.
34. M. S. Sharawi, Printed multi-band MIMO antenna systems and their performance metrics [wireless corner], *IEEE Antennas Propag. Mag.*, vol. 55, no. 5, pp. 218–232, Oct. 2013.
35. Ojaroudiparchin, N.; Shen, M.; and Pedersen, G. F. Small-size tapered slot antenna (TSA) design for use in 5G phased array applications. *Applied Computational Electromagnetics Society Journal* 2018, 32, 193-202.
36. Mazloum, J.; *et al.* Compact triple-band S-shaped monopole diversity antenna for MIMO applications. *Applied Computational Electromagnetics Society Journal* 2015, 30, 975-980.
37. Ojaroudiparchin, N.; *et al.* A switchable 3-D-coverage-phased array antenna package for 5G mobile terminals. *IEEE Antennas Wireless Propag. Lett.* 2016, 15, 1747–1750.
38. Parchin, N.O. *et al.* MM-wave phased array quasi-yagi antenna for the upcoming 5G cellular communications. *Applied Sciences* 2019, 9, 1-14.
39. Elfergani, I.T.E. *et al.* *Antenna fundamentals for legacy mobile applications and beyond*. Springer Nature 2017, pp. 1-659.
40. Ojaroudi, N. *et al.* Compact ultra-wideband monopole antenna with enhanced bandwidth and dual band-stop properties. *International Journal of RF and Microwave Computer-Aided Engineering* 2014, 346-357.
41. Ojaroudi, N. *et al.* Enhanced bandwidth of small square monopole antenna by using inverted Ushaped slot and conductor-backed plane. *Applied Computational Electromagnetics Society (ACES) Journal*. 2012, 27, 685– 690.
42. Syrytsin, I.; Zhang, S.; Pedersen, G.F. Performance investigation of a mobile terminal phased array with user effects at 3.5 GHz for LTE advanced. *IEEE Antennas and Wireless Propagation Letters* 2017, 16, 1847-1850.
43. Ojaroudiparchin, N., Shen, M., Pedersen, G.F. Design of Vivaldi antenna array with end-fire beam steering function for 5G mobile terminals. 23rd Telecommunications Forum Telfor (TELFOR), Belgrade, Serbia, 24–26 November 2015, 587–590.

44. Hussain, R. *et al.*, 4-element concentric pentagonal slot-line-based ultra-wide tuning frequency reconfigurable MIMO antenna system. *IEEE Trans. Antennas Propag.*, 2018, 66, 4282–4287.
45. Parchin, N. O, *et al.*, 8×8 MIMO Antenna System with Coupled-Fed Elements for 5G Handsets. IEEE Proceeding of Antennas and Propagation Conference. November 2019, Birmingham, UK.



© 2019 by the authors. Submitted for possible open access publication under the terms and conditions of the Creative Commons Attribution (CC BY) license (<http://creativecommons.org/licenses/by/4.0/>).